Journal of
Materials Chemistry C

PAPER

Cite this: J. Mater. Chem. C, 2016, 4, 10069

Enhancement of optical gain characteristics of quantum dot films by optimization of organic ligands†

Sidney T. Malak,[a] Evan Lafalce,[b] Jaehan Jung,[a] Chun Hao Lin,[a] Marcus J. Smith,[ac] Young Jun Yoon,[a] Zhiqun Lin,[a] Z. Valy Vardeny[b] and Vladimir V. Tsukruk*[a]

Received 25th July 2016,
Accepted 5th October 2016

DOI: 10.1039/c6tc03148j

www.rsc.org/MaterialsC

This work examines how the optimization of molecular dimensions and chemical functionality of the organic ligands of quantum dots (QDs) can be explored for dramatic enhancement of the optical properties of QD films, particularly, optical gain. We show that the replacement of traditional QD organic ligands with a much shorter ligand, butylamine, yields a dense QD-packing that results in a two-fold increase in optical gain. Overall, the highly packed QD films exhibit very large net gain values ($\sim$500 cm^{-1}) which greatly exceed typical Cd-based QD films with traditional ligands. In addition, thresholds for amplified-spontaneous emission (ASE) down to 50 $\mu J\ cm^{-2}$ were observed, which is exceptionally low for ns-pulse pumped QD systems. Our results confirm an additional route for obtaining high optical gain using QDs, and outline a strategy for modifying the optical gain characteristics by ligand exchange without needing to modify the QD selection. Consideration of the ligands along with QD compositional design could make it possible to fabricate photonic systems with exceptionally low lasing thresholds, and offers a route toward achieving high gain using steady state pumping, an extremely difficult feat to achieve in traditional QD systems.

Introduction

The large variety of nanoparticles, nanoscale deposition approaches, and nanoscale patterning strategies that have been recently introduced open up tremendous possibilities in the area of nanophotonics.[1–4] A primary advantage of nanoscale particles over conventional bulk materials is their size-and-shape dependent properties.[5–9] The tuning of nanoparticle properties is possible by carefully controlling their dimensions and shape, and allows a single nanomaterial to satisfy multiple system constraints (for example, multiple emission colors), which in a bulk scale system may require multiple materials. This tunability has led to exciting possibilities in the areas of lasers,[10,11] LEDs,[12,13] solar cells,[14] and imaging.[15]

Quantum dots (QDs) are well-known semiconducting nanoparticles with a diameter typically below 10 nm that exhibit size-dependent properties due to quantum confinement of the exciton Bohr radius.[5] QDs have attracted much attention due to their broadband absorption, narrow band emission, high quantum yield, and minimal optical loss (which continues to be an obstacle for plasmonic particles).[16] Since the degree of confinement depends on the size and material of the quantum dot, the absorption and emission can be tuned from blue to NIR,[17] with smaller QDs displaying bluer absorption/emission.[18] QDs exhibit a number of additional characteristics that make them ideal candidates for photonic applications, including: polydispersity below 10%,[19] full-width at half-maximum (FWHM) down to 30 nm,[17] quantum yields up to 90%,[20] and tunable chemical functionality and packing density *via* ligand exchanges.[21,22] Research into the underlying mechanisms behind the confinement phenomena has been enabled in large part by the development of reliable synthesis approaches for semiconducting QDs.[23,24] Furthermore, QDs are compatible with many nanoscale deposition techniques (spin-assisted layer-by-layer assembly,[25,26] Langmuir–Blodgett,[27] Langmuir–Schaefer[28]) and patterning techniques (jet printing,[29] μContact printing,[12] transfer printing,[30] photopatterning[31]), allowing for control over the arrangement of QDs and their collective behavior. This universality makes QDs ideal candidates for next generation photonic applications, including imaging and labelling,[15] solar cells,[14] LEDs,[13] and quantum computing.[32]

Quantum dots have particular potential in the area of optical gain and lasing systems. For example, gain from the blue to NIR

[a] *School of Materials Science and Engineering, Georgia Institute of Technology, Atlanta, Georgia 30332, USA. E-mail: Vladimir@mse.gatech.edu*
[b] *Department of Physics and Astronomy, University of Utah, Salt Lake City, Utah 84112, USA*
[c] *Aerospace Systems Directorate, Air Force Research Laboratory, Wright-Patterson Air Force Base, Ohio 45433, USA*

† Electronic supplementary information (ESI) available. See DOI: 10.1039/c6tc03148j

has been demonstrated using many types of QDs, including CdTe,[33] PbS,[34] CdSe,[35,36] CdSe/ZnS,[37] and CdSe/CdS/ZnS.[38] Typical gain values range from 60–200 cm^{-1} depending on the pumping conditions, system design, and type of QD.[33–38] Various feedback mechanisms for lasing have also been demonstrated, including microcapillary resonators,[35,39] microsphere resonators,[40] distributed feedback resonators,[41] and planar microcavities.[42] These studies clearly demonstrate the potential of quantum dots for optical gain and lasing applications.

To date, the majority of studies have tried to maximize optical gain by minimizing the Auger recombination rate *via* size,[43] type-I design,[11] type-II design,[44,45] and QD composition.[33–38] These studies have been complemented by investigations on the formation and relaxation dynamics of the various exciton, biexciton, and multiexciton states in different types of quantum dots (core, core/shell, core/graded shell) using state-resolved pumping/probing.[46–49] This has resulted in a steady increase in understanding of the structural dynamics of multi-excitons, and led to important discoveries like size-independent occupation thresholds and gain tailoring *via* excitonic state.[48,50] However, only a few studies have considered how QD packing density and thermodynamic properties of the film affect the optical gain characteristics.[33] This is surprising since QD packing is a particularly important area of investigation in QD photovoltaics where ligand selection has been used to increase QD packing and therefore charge transport.[22] Initial results, however, have shown that small ligand engineering can allow for ultra-high optical gain of 650 cm^{-1} to 1200 cm^{-1}.[10,51] The increase of optical gain stems from the fact that the ligand affects QD packing density (QD-loading), and, in turn QD-loading affects the stimulated emission build-up time and optical gain value (ESI:† eqn (S1) and (S2)).[5] In addition, QD-loading affects the effective refractive index of the film which affects the degree of light confinement.[5] Furthermore, tightly packed QD films with short QD ligands exhibit higher thermal transport, which is an important factor to consider for film integrity under optical pumping.[10,52] The functional groups of the ligand also control the type of bonding to the QD surface (L-type *versus* X-type) and how readily reversible adsorption/desorption occurs.[53,54] Finally, the thermodynamic properties of the ligands (melting point, vapor pressure, boiling point) can vary widely between short and long ligands,[55] which can affect the physical and optical stability of the films due to desorption of ligands, film dewetting, or rearrangements of QDs. Understanding how the QD ligand choice affects the optical gain properties is thus critical to optimize system design, and could offer new strategies for tuning the magnitude and stability of optical gain that have not been considered before.

In this work, we demonstrate how the optical gain characteristics (threshold, magnitude, and stability) of QD films depend on the type of ligand used to stabilize the QD. These results are examined from the perspective of how the size and thermodynamic properties of the QD ligand affect the physical characteristics of the film, including QD-loading fraction and refractive index. We show that replacing traditional long chain ligands with shorter ligands can increase QD-loading up to 50% and consequently increase the refractive index up to 1.88 (at 650 nm). These changes profoundly influence the emission light confinement within the film, as well as the optical gain magnitude, with more than a two-fold increase observed between the long and short QD–ligand systems. These property changes have led to exceptionally high net gain values ($\sim$500 cm^{-1}) for a Cd-based QD system, as well as excellent optical stability. This research shows a facile approach for tuning the QD gain characteristics that does not require any modification to the QD synthesis process or selection of different QDs.

Experimental

Chemicals and materials

Cadmium oxide (CdO), zinc acetate (99.99%), zinc acetylacetonate, tri-*n*-octylphosphine (TOP, 90%), selenium powder, and 1-dodecanethiol (98%) were obtained from Sigma Aldrich. Hexanes, heptane, and octylamine (OctA, 98%) were obtained from Alfa Aesar. 1-Octadecene (ODE, 90%), hexadecylamine (HDA, 90%), butylamine (BA, 98%), and oleic acid (97%) were obtained from TCI. Toluene was obtained from BDH Chemicals. The fluorinated polymer CYTOP was obtained from AGC Chemicals. All chemicals were used as received.

Preparation of core/graded shell $CdSe/Cd_{1-x}Zn_xSe_{1-y}S_y$ quantum dots

High quality oleic acid-capped red emitting core/graded shell $CdSe/Cd_{1-x}Zn_xSe_{1-y}S_y$ QDs were prepared by slightly modifying the reported method.[24,51,56,57] 1 mmol of CdO, 2 mmol of zinc acetylacetonate, 5 ml of oleic, and 25 ml of ODE were placed in a 150 ml three neck flask. The mixture was degassed at 150 °C for 1 h. The temperature was then increased to 300 °C under Ar. Subsequently, 0.2 ml of 1 M Se/TOP solution was rapidly injected to initiate nucleation and growth. After 5 min elapsed, 0.3 ml of dodecanethiol was added drop-wise. The reaction was kept at 300 °C for 20 min. Then, 1 ml of 2 M S/TOP was injected. The heating mantle was removed to stop the reaction after 10 min. 10 ml of hexanes was added when the temperature becomes 70 °C.

Ligand exchange: preparation & characterization

The ligand capping the QDs was exchanged from oleic acid (the original ligand during QD synthesis) to one of the other ligands used in this study by a multistep ligand exchange. The prepared $CdSe/Cd_{1-x}Zn_xSe_{1-y}S_y$ QDs were purified with acetone three times to remove excess oleic acid and ODE. Subsequently, oleic acid-capped $CdSe/Cd_{1-x}Zn_xSe_{1-y}S_y$ QDs were re-dispersed in hexane, and then an excess amount of the new ligand (butylamine, octylamine, or hexadecylamine) was added. The ligand exchange reaction was allowed to proceed at 45 °C for 4 hours. The solution was then precipitated using methanol and re-dispersed in a mixture of hexane and the new ligand. This procedure was repeated three times. It is worth noting that a residual amount of the original ligand is typically present after a ligand exchange so a mixture of oleic acid and the new ligand (butylamine, octylamine, or hexadecylamine) might likely exist.[22] However, the three rounds of ligand exchange should minimize this possibility to a level not easily detectable. The resulting product was finally precipitated using methanol and dispersed in the desired solvent. Proton nuclear magnetic resonance (HNMR) was used to examine how effectively the new ligand displaced the original ligand by examining changes in peak intensity, shifts in peak position, and the emergence of new peaks. Measurements were made using a Varian Mercury 400 NMR instrument with samples in deuterated chloroform.

The morphology of the core/graded shell $CdSe/Cd_{1-x}Zn_xSe_{1-y}S_y$ QDs was studied by transmission electron microscopes (JEOL 100cx (100 kV) and Tecnai F30 (300 kV)). The mass fraction of the QDs in solution was determined by analyzing the amount of mass present *versus* temperature using a thermal gravimetric analysis (TGA) instrument (TA Instruments TGA Q50) with a 100 μl open platinum pan. Samples were analyzed by first equilibrating at 30 °C followed by ramping the temperature to 600 °C using a 10 °C min^{-1} temperature profile under a constant flow of nitrogen. Volume fractions of the organic and inorganic components were calculated using the bulk density of each component.

QD–ligand film preparation

QD films were fabricated *via* spin-casting (2000 rpm, 1.5 minutes) a QD solution (heptane or toluene). Film thickness ranged from 150–250 nm in order to support only the first waveguide mode. QD films were deposited on a CYTOP film (1400–1600 nm thick) which has a sufficiently low refractive index (n_{650} = 1.34) to cause light confinement and waveguiding within the QD film.[58] The CYTOP was exposed to air or Ar plasma for 5 seconds in order to improve wetting of the CYTOP by the QDs. Silicon with a 290–295 nm thick SiO_2 surface layer was used as a substrate to minimize leakage (and attenuation) of light from the QD film. However, the attenuation of light that does leak from the QD film into the Si substrate helps ensure that the light detected at the edge of the substrate (during the gain measurement) is the light that has propagated through the QD film (and not the substrate). The substrates were cleaved to obtain sharper, cleaner edges which improve the intensity of the output light and to help ensure that the area of the film exposed to the pump light was uniform over the length of the pump strip length.

Film & solution characterization

UV-vis extinction of the QDs was collected from 350–800 nm (1 nm intervals) using a Shimadzu UV-vis-2450 spectrometer with D2 and tungsten lamps offering a wavelength range of 300–1100 nm. The photoluminescence of the films from 550–750 nm was measured using a Shimadzu RF-5301PC spectrofluorophotometer. The quantum yield of the QDs was approximated using the relative method according to outlined procedures.[59] Rhodamine 101 was used as the reference dye due to its appropriate absorption and emission overlap with the QDs used in this study.

Dark field, bright field, and photoluminescence images were collected using a Dagexcel-M Digital Firewire camera (cooled) and a 50× objective (NA: 0.80). Photoluminescence imaging was performed using excitation from a blue bandpass filter (450–490 nm) with a dichroic mirror that reflects optical wavelengths below 495 nm and with a longpass emission filter that passes optical wavelengths above 500 nm. Both filters and dichroic mirror are from Chroma Technology Corp. The light source was a quartz halogen lamp with an aluminum reflector providing an emission range of 420–850 nm and a maximum power of 150 Watts.

The QD films were examined using a spectroscopic ellipsometer from Woollam (model M2000) with a wavelength range of 245–1000 nm and a rotating compensator configuration. Film thickness was determined by applying a Cauchy model to the transparent region of the optical spectrum. The refractive index at 650 nm (also in the transparent region) was estimated with the Cauchy model. QD-loading (volume fraction) was calculated using the Bruggeman model, the effective refractive index of the film (at 650 nm), and the refractive index of the appropriate ligand. The refractive index of the $CdSe/Cd_{1-x}Zn_xSe_{1-y}S_y$ QD material was approximated using CdSe while the refractive index value of the ligands was determined from literature or supplier.

Atomic force microscopy (AFM) images were collected using a Dimension Icon AFM microscope (Bruker) in tapping mode according to the usual procedure.[60] MikroMasch pyramidal silicon tips were used for scanning.

Confinement factor modeling

Modeling of the confinement factor was done using Mode Solutions (version 7.7.786) from Lumerical Solutions Inc. The confinement factor (for the E_x component) was determined by integrating the power of the electric field over the thickness of the QD film and normalizing against the total power in the system. A 1 dimension *y*-direction solver (1DT: Z-propagation model) was used to determine the modes and electric field distributions, where the film cross-section was in the *xy*-plane and the light propagation in the *z*-direction. The theoretical layered model corresponded closely to the actual layered systems in terms of thicknesses and refractive index (the refractive index of each QD–ligand combination was obtained from an average of multiple films).

Optical gain and loss measurements and fitting

The third harmonic (355 nm) of a Spectra Physics Quanta-Ray INDI-series Pulsed Nd:YAG laser (pulse width of 5–8 ns, repetition rate of 10 Hz) was used as a seed for a GWU-Lasertechnik basiScan Beta-Barium Borate Optical Parametric Oscillator, producing a pulse of wavelength 440 nm. This wavelength of 440 nm was used for all ASE threshold, gain, and loss measurements in this study.

Variable stripe length (VSL) gain measurements were performed according to standard procedure.[78] The excitation beam was shaped into a stripe of 125 μm width using a cylindrical lens (15 cm focus length), and the stripe length was controlled by a pair of blades mounted on mechanically controlled stages that provided an adjustable slit. Only the central 10% of the beam was used to minimize pump inhomogeneity due the Gaussian intensity profile. The pump beam intensity, I_{pump}, was varied by means of a pair of polarizers or neutral density filters. One end of the stripe excitation was placed on the cleaved edge of the film while the length of the excitation stripe was progressively increased. The emission from the edge was collected with a 5 mm fiber and recorded using a commercial spectrometer (Ocean Optics USB4000; resolution 2 nm). Gain values were extracted according to the model proposed by Malko *et al.*,[39] that, in addition to the exponential gain term, incorporates a linear exciton term to account for photoluminescence. This has been a common approach for fitting QD gain.[11,33,35,51]

Loss measurements were conducted in the same experimental geometry. However, in this case, the length of the excitation stripe was held constant, while the distance of the stripe from the edge of the film, d, was varied by simultaneously varying the position of both blades.[61] As the emission propagates towards the collecting fiber, it experiences attenuation by scattering and re-absorption in the unexcited region of the film. The decay of the collected emission signal with increasing distance, d, from the edge was fit to an exponential law: $I(d) = I(0)\exp(-\alpha d)$ to extract the loss coefficient α.

Gain threshold values were obtained by determining the intersection of the linear fits to the low intensity (linear) region and the high intensity (superlinear) region of the pump fluence *versus* emission plot (on a log–log scale).

Results and discussion

Quantum dot characteristics

The quantum dots in this study have a core/graded shell type-I composition ($CdSe/Cd_{1-x}Zn_xSe_{1-y}S_y$), diameter near 8 nm, and exhibit typical broadband absorbance below 614 nm and a Stokes-shifted narrow emission peak near 624 nm (Fig. 1a). All QD films use the same type of quantum dot since the presence (and type) of inorganic passivating shell has been shown to affect exciton dynamics and gain properties.[46,48] The length of the amine-functionalized ligands was varied from 16 (hexadecylamine), 8 (octylamine), to 4 (butylamine) carbon atoms in order to examine how the maximum QD-packing density depends on the ligand length (Fig. 1b and c). Oleic acid was chosen as a standard control primarily for comparative purposes because it is a common QD ligand widely used in the literature.[10,24,45,62]

The efficiency of the ligand exchange process is monitored and confirmed *via* NMR, an example of which is shown in Fig. S1 and S2, see ESI.† The optical properties of the QDs were examined before and after the ligand exchange since the process involves exposure to multiple solvents and washing steps, as well as a change from a carboxylic functional binding group to an amine group. Quantum yield experienced the most notable change (decrease) after the ligand exchange process, with other optical properties remaining nearly unaffected (Table S1, ESI†). Decreases in quantum yield are typically attributed to less effective passivation of the QD surface which opens up nonradiative relaxation pathways for exciton recombination.[53,63,64] However, in this case the variation in QY should not be a critical factor since the stimulated emission lifetime of these QD films (less than 0.1 ns) (Table S2, ESI†) is much shorter than typical alloyed QD spontaneous recombination lifetimes (<4 ns).[63,64]

QD film uniformity & morphology

QD films were fabricated *via* spin-casting, covering the substrates uniformly and having uniform PL emission (Fig. 1a inset), as evidenced by bright field, dark field, and photoluminescence imaging (Fig. S3, ESI†). The QD films were deposited on a fluorinated polymer layer (CYTOP) with a low refractive index to improve light confinement (waveguiding) within the QD film.[51,58] The CYTOP film was briefly exposed to plasma in order to promote wide-spread wetting by the QD film. AFM topographical and phase images show that the morphology of the QD films depends on the ligand coating the QDs. Films of oleic acid capped QDs (oleic–QD) show the presence of domains with a dense arrangement of QDs (Fig. 2a). The phase image indicates that the QD domains are separated from

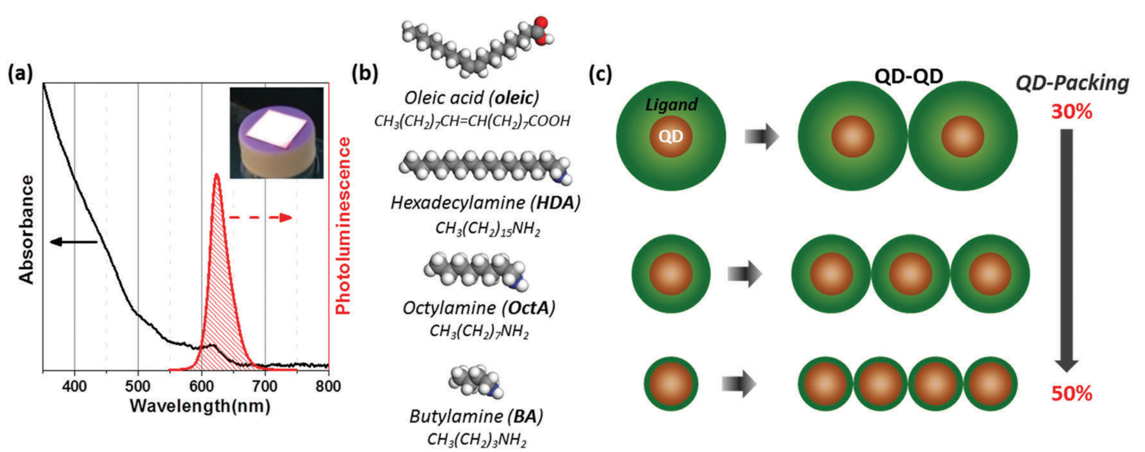

Fig. 1 The QDs show broadband absorption and narrowband emission (a), which is easily visible under UV excitation (Inset). Ligands of different size (b) were used to stabilize the QDs in order to control the spacing between adjacent QDs when deposited into film (c). The QD–QD spacing dictates the maximum QD-packing density.

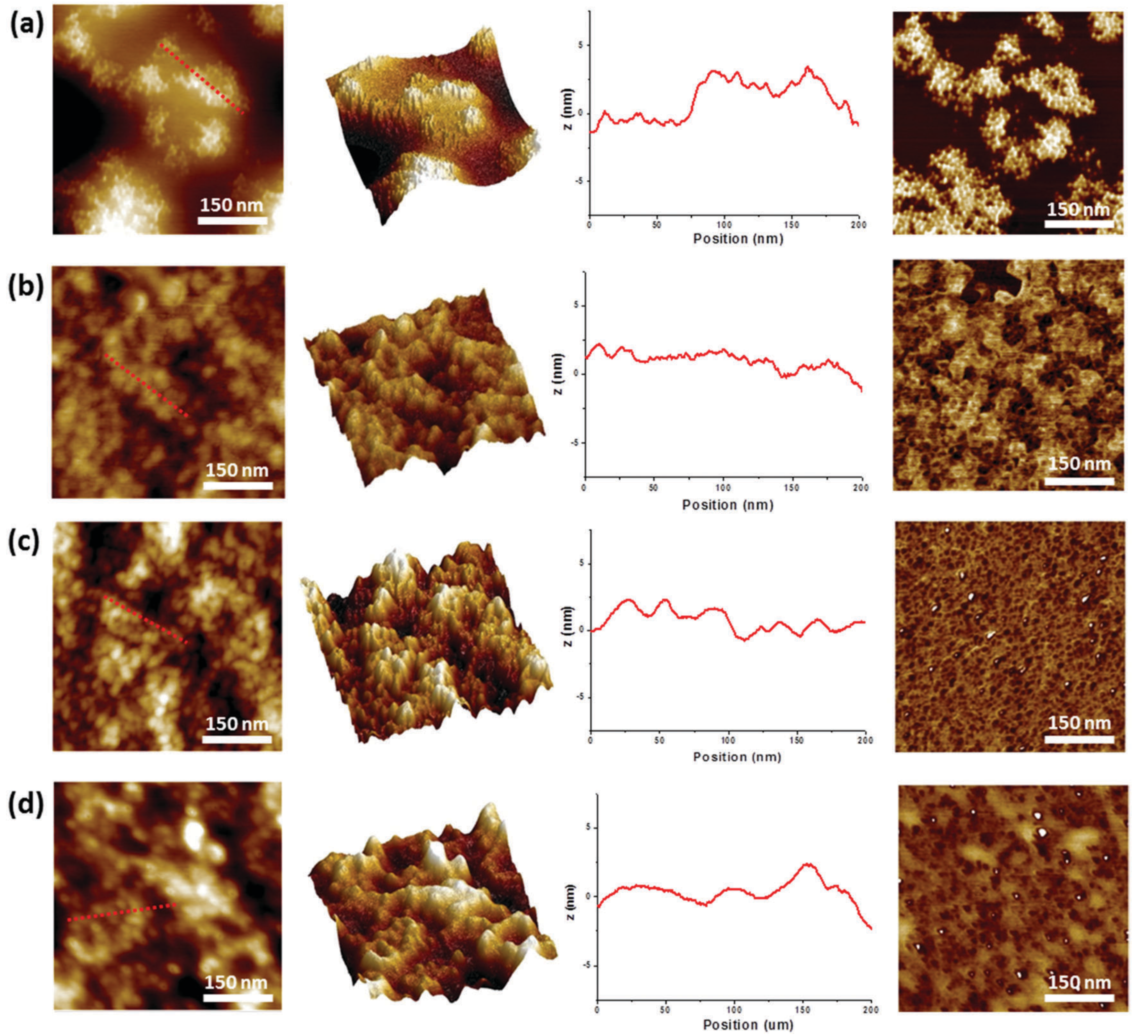

Fig. 2 AFM surface morphology (column 1), 3D topography projection (column 2), topographical cross-section (column 3), and phase (column 4) for (a) oleic acid, (b) hexadecylamine, (c) octylamine, and (d) butylamine capped QD films. *Z*-scale is 20 nm for the oleic–QD film scan and 10 nm for all others. Phase scale is 20° for the oleic–QD film scan and 10° for all others.

adjacent QD domains by regions of a different phase which is likely excess oleic acid that was not removed during washing as well as a thick coating of oleic acid from submerged QDs.

The QD films of hexadecylamine-capped QDs (HDA–QD), octylamine-capped QDs (OctA–QD), and butylamine-capped QDs (BA–QD) have larger particle-like domains (likely aggregated QDs) that appear to cover the entire surface area (Fig. 2b–d). The formation of localized lattice-like regions has been observed previously in oleic acid–QDs films, as well as the transformation to a more chaotic pattern upon replacement with a shorter ligand like butylamine.[22] We attribute the presence of a lattice arrangement in the oleic–QD film and the tighter aggregate arrangement in the BA–QD, OctA–QD, and HDA–QD films to two factors.

First, oleic acid provides exceptional colloidal stability due to its covalent bond with the QD surface and large size, which reduces aggregation of QDs in solution and allows for deposition of individual QDs that can form uniform QD lattice domains during spin-casting. On the other hand, the QD colloidal stability provided by the amine-based ligands (BA, OctA, HDA) is not as effective, which can lead to minor QD aggregation in solution that leads to larger domains in the film state. Second, the volume of oleic acid is greater than all the amine functionalized ligands (discussed later), which leads to greater spacing between QDs in the film state than that provided by the smaller amine-ligands. Greater QD spacing makes it easier for lattice-like QD arrangements to be observed.

Cross-sections of the height scans show a surface with sub-nanometer high bumps, indicating that the QDs are tightly packed with the free ligand filling the areas between adjacent QDs. The R_q roughness spans from approximately 4 nm (500 nm scan area) to 8 nm (10 μm scan area) for all samples. In some instances, BA–QD films will appear smooth with no clear indication of QDs if examined very soon after film deposition, which is likely due to the fluid-like nature of butylamine at room temperature (melting point of −49 °C in free state) and its volatility (vapor pressure of 82 mmHg).[55] This fluid nature can compromise the AFM scanning to track surface features.

Ligand characteristics & QD-loading (volume fraction)

The four ligands used in this study each have a different molecular volume in the free-state (oleic acid: 0.320 nm^3, HDA: 0.295 nm^3, OctA: 0.159 nm^3, BA: 0.091 nm^3).[55] Therefore, changing the ligand may change the maximum allowable QD-packing density (volume loading) in QD films, which could impact the magnitude and threshold of optical gain.

The QD-packing density was monitored using a variety of approaches. High-resolution TEM (HR-TEM) of drop-cast QD films shows that the space between QDs decreases as the size of the ligand is decreased, with oleic–QDs having the largest QD spacing and BA–QDs having the smallest (Fig. 3a). In addition, QD content was estimated using ellipsometry (see Experimental section).[51] Examination of multiple films for each type of ligand–QD film agrees with the trend observed in HR-TEM, with QD-loading (volume percent) ranging from approximately 30% for oleic–QD films to 50% for the BA–QD films (Fig. 3b). A similar increase in density of QD films has been observed previously upon exchanging oleic acid for butylamine (before film deposition).[22] The observed trend between ligand size and QD-loading follows the theoretical relationship between QD-loading and ligand size, which predicts 40% face-centered-cubic (FCC) loading for oleic–QD and 50% for BA–QD (no unbound ligand is present in the film) (Fig. S4, ESI†).

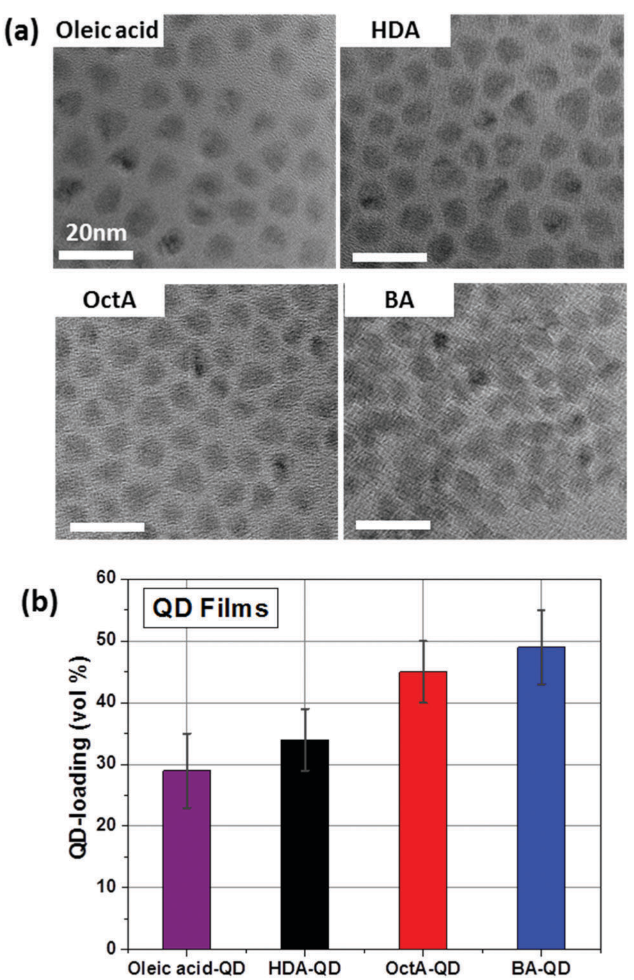

Fig. 3 Four ligands of different size were used in order to examine how QD-packing is affected by ligand size. (a) HR-TEM micrographs of drop-cast QD solutions and (b) ellipsometry characterization of spin-cast QD films show that reducing the size of the ligand increases the QD-loading (packing density) of QDs in films. Scale bar is 20 nm for all TEM micrographs.

Finally, TGA of drop-cast QD films shows that the amount of organic material (excess ligand and bound ligand) present in the QD solutions generally decreases for shorter ligands (Fig. S5, ESI†), which corroborates the trend seen in HR-TEM and ellipsometry. Differences in the specific QD volume fraction between the spin-cast QD films and drop-cast QD films can be attributed to the difference in deposition methods, as well as the volatility of the ligands (Fig. S5, ESI†).[55,65,66]

QD packing is a critical characteristic since optical gain is proportional to QD volume fraction.[5] For example, an increase of QD packing from 30% to 45% (factor increase of 1.5) is expected to cause a similar 1.5 factor increase in the magnitude of optical gain (ESI,† eqn (S1)). In addition, QD packing affects the film refractive index, which affects the degree of light confinement within the QD film, the number of waveguide modes, and the optical loss due to leakage of light during propagation.[67] A higher film refractive index increases the index contrast with the underlying material (CYTOP) and increases light confinement within the film, a necessary condition for achieving high optical gain.

Optical gain threshold, magnitude, & stability

The existence of ASE is supported by a number of emission characteristics such as the presence of clear threshold behavior in emission intensity *versus* excitation intensity plots.[11,45,68] At threshold, the emission dependence on the pump excitation intensity transitions from approximately linear at low intensity to super-linear at successively higher pump fluence, as was clearly observed for all QD samples (Fig. 4a) (note both axes are log scale). ASE threshold values were obtained by determining at what fluence this transition occurs (Fig. S6, ESI†). The light-light curves were quite consistent over multiple spots (Fig. S7, ESI†). The BA–QD, OctA–QD, and HDA–QD films exhibited thresholds of approximately 30–50 μJ cm^{-1}[2] which matches many of the lowest QD film thresholds to date,[10,11] and is 5–10 times lower than the threshold of typical drop-cast QD films using traditional ligands.[45,68] The exceptionally low thresholds are attributed to the uniformity of the QD films and the high QD-packing density, which allow for efficient light generation and propagation. Furthermore, the core/graded shell composition of the QD also plays an important role, with previous studies showing that a graded shell imparts very effective surface passivation of the core. This passivation decouples the core exciton states from surface trap states, effectively deactivating the non-radiative surface trap relaxation pathway.[46,69]

ASE threshold indicates the point where optical gain and loss are equal, and can depend on a number of factors.[70] In this case, the large differences in threshold are attributed primarily to the nature of the physical and thermal properties of the

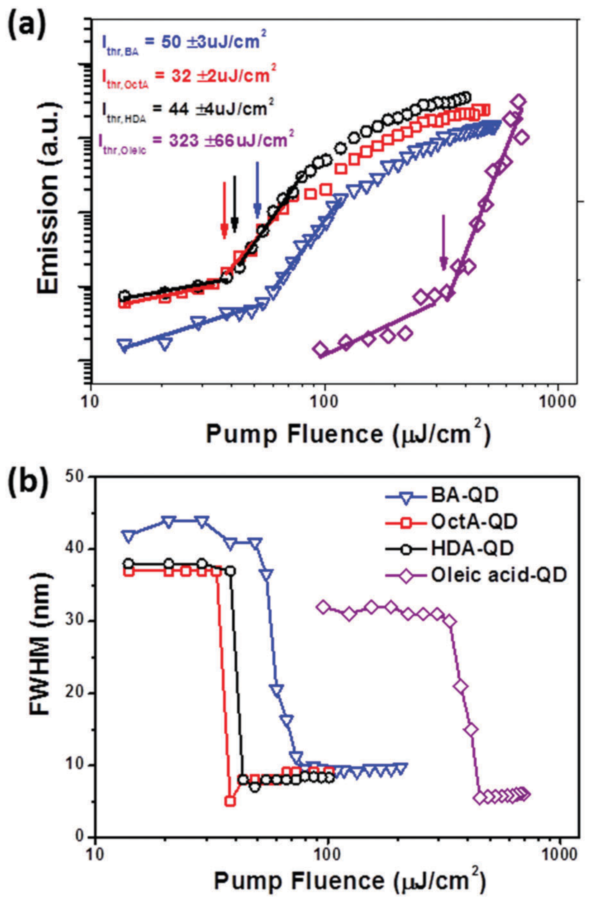

Fig. 4 ASE in the QD films is identified by multiple characteristics of QD emission as the QD film is pumped with different excitation powers. (a) Emission intensity (log–log, scaled for clarity) showing threshold behavior, and (b) full-width at half-maximum (FWHM) of the emission peak showing spectral narrowing.

ligand. All ligands with the alkane structure and amine functionalization (butylamine, octylamine, and hexadecylamine) have similar thresholds, which are also much lower than that shown by the film with the oleic acid ligand (which has an internal double bond and a carboxylic acid terminal group). The internal double bond makes oleic acid waxy at room temperature and therefore highly fluid under optical pumping. This fluidity allows for more QD diffusion, which can lead to QD aggregation that increases optical scattering (optical loss) and modifies the localized refractive index (disrupts light propagation), both of which would delay the onset of ASE (increase the threshold). Furthermore, the waxy nature makes oleic acid QD films highly susceptible to physical damage.

The functional group of the ligand could play a role as well by imparting different degrees of surface passivation to the QD, which has been shown to have an impact on exciton trapping rates and the required average exciton gain threshold.[46,71] Auger recombination (an important obstacle for achieving QD optical gain) has also been shown to depend on factors like charged exciton states that could be influenced by the ligand functional group.[72,73] In addition, non-radiative hole relaxation has been shown to occur through a non-adiabatic ligand-mediated mechanism, which means different ligands could increase or decrease this non-radiative pathway.[74] However, this phenomenon is hindered by the presence of an inorganic shell so it is not likely to be an important factor for the core/graded shell QDs in this study. Likewise, it has also been shown that the Auger recombination rate can, in certain instances, be relatively independent of surface passivation.[75] So, at this point in time it is unclear how intrinsic exciton dynamics are affected by the ligand choice and its influence on ASE threshold.

Spectral narrowing of the emission peak occurs simultaneously with threshold behavior and is an additional critical indication of the ASE phenomenon.[11,68] The FWHM of PL of all samples was approximately 30–40 nm, but narrowed to around 10 nm once ASE emerged (Fig. 4b), which is common for QD ASE.[11,68] All films show similar spectral narrowing (78 $\pm$ 3% reduction) compared to their initial PL FWHM. However, the QD film with the oleic acid ligand (carboxylic acid functionality) displayed the narrowest ASE FWHM (6 nm) since it began with the narrowest PL FWHM (32 nm). The QD films with amine functionalized ligands all show similar spectral narrowing to a FWHM of 11 nm (from $\approx$40 nm). The difference in PL FWHM appears to be correlated with how well the QDs are physically arranged and the chemical functionality of the ligand. As shown previously, the oleic acid–QD film has domains of well-ordered QDs while the amine-QD films (BA–QD, OctA–QD, and HDA–QD) have a less ordered arrangement (Fig. 2). These differences could affect the degree of optical scattering during light propagation (and therefore the broadening of PL FWHM). In addition, the chemical functionality of the ligand can affect QD surface passivation which affects the emission position, quantum yield, and electronic structure of the QD surface.[76] Additional confirmation of ASE is provided by the 10–15 nm red-shift of the ASE peak compared to the PL peak. This is a common trait of ASE often attributed to interparticle electronic energy transfer and optical re-absorption (Fig. S8, ESI†).[68,77]

The direct quantitative measurement of optical gain for each film was obtained using the variable stripe length (VSL) pumping approach, which involves optical excitation of the film using an excitation strip of variable length (Experimental, Fig. 5a and b).[78] If positive net gain is achieved, the spectrally narrowed ASE peak will emerge as the pump length is increased and the emission will exhibit an exponential increase of intensity as the optical pump strip is lengthened (Fig. 5a and b).[33–35]

Optical gain appears to scale with QD-packing (for the same ligand functional group), with the HDA–QD film displaying modest gain (225 $\pm$ 53 cm^{-1}) similar to that reported in the literature for Cd-based QD films.[33,68] In contrast, the OctA–QD and BA–QD films exhibit the highest gain (518 $\pm$ 49 cm^{-1} and 508 $\pm$ 113 cm^{-1}, respectively) (Fig. 6a). The OctA–QD and BA–QD films have similar gain values because in this case the films had similar QD-loading (50% and 49%, respectively), indicating that QD-loading is affected by both ligand length and the washing process. Gain values were averaged from multiple spots over a sample (Fig. S9, ESI†).

These gain values exceed typical QD gain values (60–200 cm^{-1}) due to the exceptionally high QD-loading,[33–35,37,38] approaching

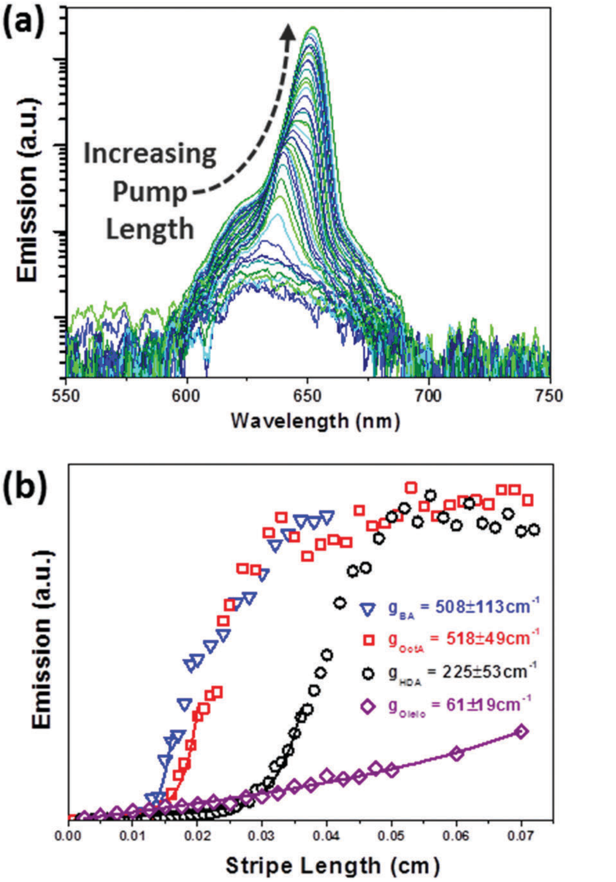

Fig. 5 The optical characteristics of the QD films were determined using the variable strip length (VSL) method. (a) Emission of an OctA–QD film (log-intensity) at various pump strip lengths. The emergence of ASE is indicated by narrowing of the emission peak. (b) Emission intensity *versus* pump length for various QD–ligands (curves were off-set for clarity). The intensity data was fit to determine the gain value (I_{pump} = 200 μJ cm^{-2}).

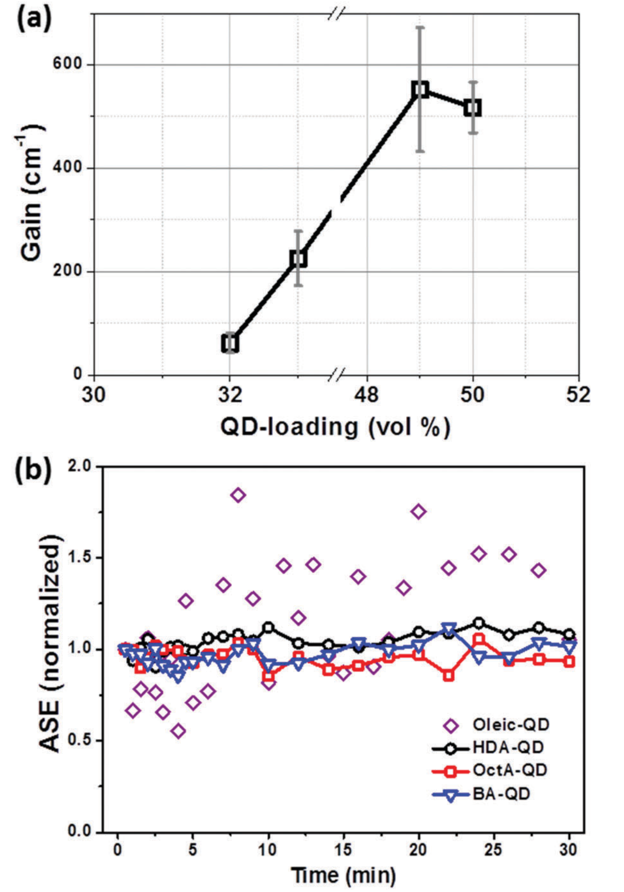

Fig. 6 The magnitude and stability of optical gain depends on the type of QD–ligand pairing. (a) Optical gain *versus* QD-packing density. QD films with higher QD-packing exhibit higher optical gains. (b) Stability of ASE over a 30 minute period.

some of the highest values reported.[36] Although, as we suggest, the high optical gain is primarily a result of QD-loading, a number of additional system characteristics play a role. These factors include reduced surface trapping and Auger recombination due to the core/graded shell QD interface,[24,46] strong light confinement due to the incorporation of a sub-cladding layer with a very low refractive index, and increased absorption of the pump beam caused by the use of a reflective substrate.[51] An oleic acid QD film displayed a low optical gain (61 ± 19 cm^{-1}) that was difficult to reliably measure due to its fluctuating ASE but was included as a reference sample since oleic acid is a commonly used QD ligand (discussed below).

The difference in optical gain magnitude between the films with different ligand–QD combinations can be attributed to a number of factors. First, as mentioned above, the material gain value is expected to depend on the QD packing density (eqn (S1), ESI†)[5] due to an increase in the density of optically excited QDs that participate in the ASE process as well as an increase in the optical density of the film. An increase of optical gain due to higher QD packing density has been observed experimentally in layer-by-layer systems.[33] For example, the increase of QD packing from the HDA-capped QD film (34%) to the BA-capped QD film (49%) can explain a factor increase of 1.44 for the gain, which accounts for a portion of the differences between these films (factor of 2.3).

Second, gain depends on the degree of light confinement exhibited by the film since efficient light confinement leads to more stimulated emission within the film, as well as lower propagation losses from light leakage into adjacent layers. Light confinement depends primarily on film thickness and refractive index (RI) contrast between the QD film and the surrounding layers, with higher refractive index contrast leading to more efficient light confinement. Refractive index contrast was dictated by the RI of the QD film since the underlying material was always CYTOP (n = 1.34) and the top layer always air. Reducing the molecular dimensions of the ligands increases QD-loading which increases the RI of the film (since QDs have a higher refractive index than the ligand).

For example, the OctA–QD and BA–QD films had the highest refractive index of all the films (1.86 ± 0.05 and 1.88 ± 0.06, respectively) near the propagation wavelength (630–650 nm). On the other hand, the oleic–QD and HDA–QD films had the lowest refractive index (1.72 ± 0.04 and 1.76 ± 0.05, respectively).

The resulting degree of light confinement can be quantified by the confinement factor (Γ), which is a measure of the power of the *E*-field confined to the QD film *versus* the power of the *E*-field present within the entire system.[10] Higher confinement factors indicate greater localization of light within the QD film and an increase of modal gain ($g_{\text{modal}} = \Gamma \times g_{\text{material}}$).[10] Modeling of the confinement factor for each of the ligand systems for various thicknesses shows that the BA–QD film can exhibit a confinement factor up to 1.7 times that shown by the oleic–QD films and 1.4 times that exhibited by the HDA–QD films for relevant thicknesses (Fig. S10, ESI†). In addition, the refractive index and thickness of the QD film determines the number and type of waveguiding modes, which affects propagation losses and might increase waveguiding efficiency. Therefore, all samples were designed to support only one waveguide mode by ensuring that the film thickness was above the first critical waveguiding thickness ($t_{c,1}$) but below the next highest critical waveguiding thickness ($t_{c,2}$) (Fig. S11, ESI†).[67]

Third, the arrangement of QDs within the film (lattice-like, aggregated, or intermittently spaced) can affect how light propagates through the film, either through the introduction of scattering sites, QD–QD coupling,[77] or transverse localization effects.[79] Optical losses associated with scattering (and re-absorption) are examined later. Fourth, thermal transport (and dissipation) depends on the length of the QD ligand and has been shown to be an important factor in QD gain systems due to thermal mediated Auger recombination.[10,52,80] Finally, the difference in gain value between the oleic–QD and HDA–QD film could be due in part to the chemical functionality of the ligands since these films have similar QD-loading and refractive index. The chemical functionality of the ligand has been shown to affect QD surface passivation, which in turn affects the quantum yield and electronic structure of the QD surface and trapping rates.[71,76] The Auger recombination rate could also play a role, although previous studies have shown the Auger recombination rate is more strongly dependent on other factors like the QD core–shell interface and volume than surface passivation.[74,81] The combination of these factors likely contributes to the difference in optical gain values that can be obtained from QD films and indicates that the type of ligand on the QD surface can strongly impact optical gain a number of ways.

Photostability of the QD films

The stability of ASE was examined over a period of 30 minutes for each type of QD film (Fig. 6b). The QD films with amine functionalized ligands (HDA–QD, OctA–QD, BA–QD) display very stable ASE, which is an indication of the stable physical and thermal characteristics of the films under pumping. The stability of each ligand–QD combination can be explained by considering the interplay between QD-loading, the thermodynamic properties of the ligands, and the thermal transport/dissipation of the film. In general, stable ASE will arise if QD mobility is minimized since mobility/rearrangement of QDs during optical pumping can lead to the formation of scattering sites (which increase optical loss) in the film, as well as alter the effective refractive index (which can affect light propagation). In addition, ASE will be more stable if heat dissipation is efficient since localized heating of the film can lead to dissociation of the ligands from the QD surface (which results in loss of QD surface passivation), and to more efficient Auger recombination (which also increases intrinsic optical loss).[80]

It is worth noting that the HDA ligand is relatively long so it yields films with relatively low QD-loading (34%) and only moderate thermal conductivity (near 0.25 W m^{-1} K^{-1}).[52] However, the HDA–QD films show stable ASE, which suggests the solid state of HDA (melting point of 45 °C) and its low vapor pressure ($\approx$0 mmHG at 25 °C) are the strongest factors.[55] On the other hand, butylamine seems to derive its ASE stability from its high QD packing (49%) and higher thermal conductivity (1.5$\times$ higher than oleic–QD),[52] rather than its low melting point (−49 °C) or high vapor pressure (8 mmHG at 25 °C).[55] In fact, it is somewhat surprising that BA–QD films exhibit such stable ASE given the volatile nature of butylamine. It is likely that desorption of weakly bound BA occurs very quickly during spin-casting and storage so that by the time gain measurements are conducted there is minimal loosely bound BA to desorb during the optical pumping process. On the other hand, apart from its low vapor pressure ($\approx$0 mmHG at 25 °C) oleic acid is a poor choice for imparting optical stability due to the low QD-loading (29%), moderate thermal conductivity (near 0.25 W m^{-1} K^{-1}),[52] and its relatively low melting point (14 °C) due to the double bond in its structure. These characteristics could allow for significant QD mobility and thermal modification of the ligands when the QD films are optically pumped, which manifest in the widely fluctuating ASE. These results show that the QD ligand is an important factor to consider in terms of optical gain magnitude and stability.

Optical loss

The intrinsic optical loss of the films was also measured to determine whether loss can account for differences in the gain values. Optical loss is determined by measuring the attenuation of ASE over different propagation distances (Fig. 7).[61] Greater attenuation of ASE occurs as the distance travelled by the light to the edge of the sample increases. Attenuation of ASE is clearly evident in the spectra for all films and is shown for the HDA-capped QD film (Fig. 7a). All amine films exhibit an exponential decrease in emission as the collective distance is increased (Fig. 7b), as expected for films that exhibit optical loss. Loss values are averaged from multiple spots (Fig. S12, ESI†).

The optical loss is observed to be proportional to the QD-loading of the film, with the HDA–QD film (lowest QD-loading) exhibiting the lowest loss (60 ± 19 cm^{-1}) and the BA–QD and OctA–QD films (highest QD-loading) exhibiting the highest loss (82 cm^{-1}) (Fig. 7c). It is difficult to judge the magnitude of these QD loss values since optical loss is often overlooked in gain studies on QD films.

However, these optical loss values are similar (within a factor of 2) to those exhibited by conjugated polymers films.[61] The scaling of loss with QD-loading is not surprising since optical re-absorption (an important component of optical loss) is proportional to QD-loading since the emitted light

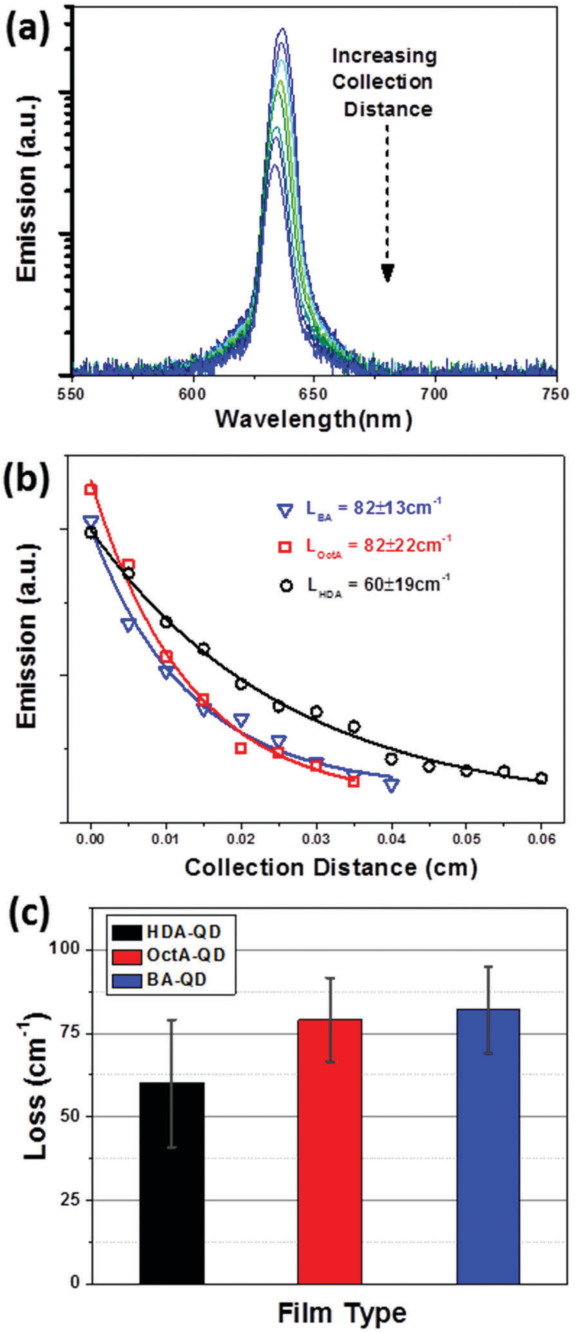

Fig. 7 (a) Typical emission spectra from the variable attenuation length method for a HDA–QD film (log intensity). (b) Optical loss fitting for the HDA–QD, OctA–QD, and BA–QD films shows an exponential decrease with collection length. (c) Optical loss for different QD–ligand films.

encounters more QDs (for a given distance) as it propagates through the film. In fact, the predicted loss for the BA–QD and OctA–QD films (scaled against the HDA–QD loss) falls within ±5% of the measured values, well within the measured standard deviations. The unstable nature of ASE for the oleic–QD film made measuring loss unreliable (Fig. 6b). These results suggest that optical loss is not the primary factor underlying the observed trends in gain *versus* QD-loading since the films with highest optical loss still displayed the highest net optical gain.

Ligand selection

The ideal ligand depends on the relative importance of gain threshold, FWHM, magnitude, and stability, as well as optical loss. Aliphatic amine functionalized ligands (butylamine, octylamine, hexadecylamine) were shown to provide lower gain threshold than that provided by oleic acid (internal double bond and carboxylic acid functionalization), while the narrowest FWHM of ASE was obtained using oleic acid (presumably due to the well-ordered physical domains). On the other hand, shorter ligands can result in higher QD-loading (which increases the number of optically stimulated QDs) and higher refractive index (which increases the confinement factor), both of which result in proportional increases to optical gain.

Obtaining stable ASE is slightly more complex, but generally requires very tight QD packing, good thermally stability (high melting and boiling points, low vapor pressure), and high thermal transport/dissipation. Unfortunately, these characteristics are not always independent, as seen with short organic ligands that offer high QD packing and large thermal dissipation,[52] but which typically exhibit low melting and boiling points and high volatility (and *vice versa*).[55] Predicting the relative impact of these factors is difficult. Finally, optical loss scales closely to QD-loading (neglecting losses associated with the presence of physical defects, surface roughness, and waveguiding losses).

Additional considerations when choosing a ligand include the colloidal stability imparted to the QDs in solution. Oleic acid typically provides very good colloidal stability due to its strong covalent bonding to the QD surface (X-type ligand).[53,54] However, amine functionalized ligands (butylamine, octylamine, hexadecylamine) form a coordinate bond to the QD surface (L-type ligand) that leads to reversible adsorption/desorption from the QD surface.[53,54] The desorption of ligands can lead to colloidal instability (aggregation of QDs) which causes scattering sites to form in the QD film during deposition and a lower than expected optical gain. QD instability was observed to be more pronounced for shorter ligands like butylamine than for longer ligands like octylamine or hexadecylamine. Therefore, the length of time before the colloidal QDs are deposited into films should factor into the choice of ligand.

Conclusions

This work demonstrates how the molecular dimensions and functionality of the ligand capping the QD affects film morphology, QD-packing density, refractive index, and the resulting optical gain characteristics. Specifically, this work shows that changing the ligand greatly affects the factors that control light propagation in the film (refractive index and refractive index contrast). Furthermore, the ligand affects QD-packing density, which has a direct effect on optical gain. Finally, evidence was provided that the chemical structure and physical and thermal properties of the ligand affect ASE threshold. The combination of these factors resulted in a 2.25 fold increase in optical gain between the lowest and highest QD-packed films (with the same functional group), with the highest QD-packed films exhibiting exceptionally high net gain values ($\approx$500 cm^{-1}). Reductions in ASE threshold and improvements in optical stability were also observed when switching from the commonly used waxy, large ligand oleic acid to the amine-functionalized ligands.

These findings outline a simple but significant strategy for altering optical gain that does not require modification to the synthesis approach or composition of the QDs. This approach allows for significant improvements in optical gain characteristics (5$\times$ reduced threshold, 2.25$\times$ increased magnitude, improved stability) *via* simple post-synthesis modification of the QD ligand. Furthermore, this approach should be compatible with any type of QD, representing a significant departure from previous studies on increasing QD gain through a sole focus on QD composition. This work is important for those interested in developing QD systems that exhibit exceptionally stable, high magnitude optical gain QD systems. Consideration of the proper ligands along with QD compositional design could offer a route toward obtaining high optical gain using steady state pumping, a major obstacle in current QD systems.

Further work should examine whether the chemical functionality of the ligand may affect QD Auger recombination rates in core/graded shell QDs, a characteristic that has a profound impact on optical gain in QD films. Furthermore, additional investigation could examine whether QD packing affects the formation and relaxation dynamics of exciton, biexciton, and multi-exciton states through the use of state-resolved pump/probe transient techniques. This could have important implications in increasing gain bandwidth and further reducing gain thresholds.[47]

Acknowledgements

Financial support is acknowledged from the Air Force Office of Scientific Research FA9550-14-1-0037 (Synthetic photonics multidisciplinary university research initiative, synthesis, fabrication and development). M. J. Smith would like to acknowledge the Science, Mathematics and Research for Transformation (SMART) scholarship funded by OSD-T&E (Office of Secretary Defense-Test and Evaluation), Defense–Wide/PE0601120D8Z National Defense Education Program (NDEP)/BA-1, Basic Research, SMART Program office Grant Number N00244-09-1-0081.

References

1 D. V. Talapin, J. S. Lee, M. V. Kovalenko and E. V. Shevchenko, *Chem. Rev.*, 2010, **110**, 389–458.
2 M. S. Tame, K. R. McEnery, S. K. Oezdemir, J. Lee, S. A. Maier and M. S. Kim, *Nat. Phys.*, 2013, **9**, 329–340.
3 B. D. Gates, Q. B. Xu, M. Stewart, D. Ryan, C. G. Willson and G. M. Whitesides, *Chem. Rev.*, 2005, **105**, 1171–1196.
4 A. Biswas, I. S. Bayer, A. S. Biris, T. Wang, E. Dervishi and F. Faupel, *Adv. Colloid Interface Sci.*, 2012, **170**, 2–27.
5 S. Hoogland, Optical gain and lasing in colloidal quantum dots, *Colloidal Quantum Dot Optoelectronics and Photovoltaics*, Cambridge University Press, 2013.
6 H. Ko, S. Singamaneni and V. V. Tsukruk, *Small*, 2008, **4**, 1576–1599.
7 Y. N. Xia, P. D. Yang, Y. G. Sun, Y. Y. Wu, B. Mayers, B. Gates, Y. D. Yin, F. Kim and Y. Q. Yan, *Adv. Mater.*, 2003, **15**, 353–389.
8 X. H. Huang, I. H. El-Sayed, W. Qian and M. A. El-Sayed, *J. Am. Chem. Soc.*, 2006, **128**, 2115–2120.
9 C. Hanske, M. Tebbe, C. Kuttner, V. Bieber, V. V. Tsukruk, M. Chanana, T. A. F. Koenig and A. Fery, *Nano Lett.*, 2014, **14**, 6863–6871.
10 M. M. Adachi, F. Fan, D. P. Sellan, S. Hoogland, O. Voznyy, A. J. Houtepen, K. D. Parrish, P. Kanjanaboos, J. A. Malen and E. H. Sargent, *Nat. Commun.*, 2015, **6**, 8694.
11 C. Dang, J. Lee, C. Breen, J. S. Steckel, S. Coe-Sullivan and A. Nurmikko, *Nat. Nanotechnol.*, 2012, **7**, 335–339.
12 A. Rizzo, M. Mazzeo, M. Palumbo, G. Lerario, S. D'Amone, R. Cingolani and G. Gigli, *Adv. Mater.*, 2008, **20**, 1886.
13 B. S. Mashford, M. Stevenson, Z. Popovic, C. Hamilton, Z. Q. Zhou, C. Breen, J. Steckel, V. Bulovic, M. Bawendi, S. Coe-Sullivan and P. T. Kazlas, *Nat. Photonics*, 2013, **7**, 407–412.
14 X. Xin, B. Li, J. Jung, Y. J. Yoon, R. Biswas and Z. Lin, *Part. Part. Syst. Charact.*, 2015, **32**, 80–90.
15 I. L. Medintz, H. T. Uyeda, E. R. Goldman and H. Mattoussi, *Nat. Mater.*, 2005, **4**, 435–446.
16 J. B. Khurgin, *Nat. Nanotechnol.*, 2015, **10**, 2–6.
17 N. Gaponik, S. G. Hickey, D. Dorfs, A. L. Rogach and A. Eychmüller, *Small*, 2010, **6**, 1364–1378.
18 V. I. Klimov, *Annu. Rev. Phys. Chem.*, 2007, **58**, 635–673.
19 D. V. Talapin, A. L. Rogach, A. Kornowski, M. Haase and H. Weller, *Nano Lett.*, 2001, **1**, 207–211.
20 A. B. Greytak, P. M. Allen, W. Liu, J. Zhao, E. R. Young, Z. Popovic, B. J. Walker, D. G. Nocera and M. G. Bawendi, *Chem. Sci.*, 2012, **3**, 2028–2034.
21 R. E. Bailey, A. M. Smith and S. M. Nie, *Phys. E*, 2004, **25**, 1–12.
22 C. Y. Kuo, M. S. Su, C. S. Ku, S. M. Wang, H. Y. Lee and K. H. Wei, *J. Mater. Chem.*, 2011, **21**, 11605–11612.
23 C. B. Murray, D. J. Norris and M. G. Bawendi, *J. Am. Chem. Soc.*, 1993, **115**, 8706–8715.
24 J. Jung, C. H. Lin, Y. J. Yoon, S. T. Malak, Y. Zhai, E. L. Thomas, V. Vardeny, V. V. Tsukruk and Z. Lin, *Angew. Chem., Int. Ed.*, 2016, **55**, 5071–5075.
25 D. Zimnitsky, C. Y. Jiang, J. Xu, Z. Q. Lin, L. Zhang and V. V. Tsukruk, *Langmuir*, 2007, **23**, 10176–10183.
26 D. Zimnitsky, C. Jiang, J. Xu, Z. Lin and V. V. Tsukruk, *Langmuir*, 2007, **23**, 4509–4515.
27 A. Gole, N. R. Jana, S. T. Selvan and J. Y. Ying, *Langmuir*, 2008, **24**, 8181–8186.

28 H. Bourvon, S. Le Calvez, H. Kanaan, S. Meunier-Della-Gatta, C. Philippot and P. Reiss, *Adv. Mater.*, 2012, **24**, 4414–4418.
29 B. H. Kim, M. S. Onses, J. B. Lim, S. Nam, N. Oh, H. Kim, K. J. Yu, J. W. Lee, J.-H. Kim, S.-K. Kang, C. H. Lee, J. Lee, J. H. Shin, N. H. Kim, C. Leal, M. Shim and J. A. Rogers, *Nano Lett.*, 2015, **15**, 969–973.
30 T.-H. Kim, K.-S. Cho, E. K. Lee, S. J. Lee, J. Chae, J. W. Kim, D. H. Kim, J.-Y. Kwon, G. Amaratunga, S. Y. Lee, B. L. Choi, Y. Kuk, J. M. Kim and K. Kim, *Nat. Photonics*, 2011, **5**, 176–182.
31 S. T. Malak, J. Jung, Y. J. Yoon, M. J. Smith, C. H. Lin, Z. Lin and V. V. Tsukruk, *Adv. Opt. Mater.*, 2016, **4**, 608–619.
32 H.-A. Engel and D. Loss, *Science*, 2005, **309**, 586–588.
33 J. Roither, S. Pichler, M. V. Kovalenko, W. Heiss, P. Feychuk, O. Panchuk, J. Allam and B. N. Murdin, *Appl. Phys. Lett.*, 2006, **89**, 111120.
34 V. Sukhovatkin, S. Musikhin, I. Gorelikov, S. Cauchi, L. Bakueva, E. Kumacheva and E. H. Sargent, *Opt. Lett.*, 2005, **30**, 171–173.
35 M. A. Petruska, A. V. Malko, P. M. Voyles and V. I. Klimov, *Adv. Mater.*, 2003, **15**, 610–613.
36 V. I. Klimov, A. A. Mikhailovsky, S. Xu, A. Malko, J. A. Hollingsworth, C. A. Leatherdale, H. J. Eisler and M. G. Bawendi, *Science*, 2000, **290**, 314–317.
37 Y. Chan, J. S. Steckel, P. T. Snee, J. M. Caruge, J. M. Hodgkiss, D. G. Nocera and M. G. Bawendi, *Appl. Phys. Lett.*, 2005, **86**, 073102.
38 J. Jasieniak, I. Fortunati, S. Gardin, R. Signori, R. Bozio, A. Martucci and P. Mulvaney, *Adv. Mater.*, 2008, **20**, 69–73.
39 A. V. Malko, A. A. Mikhailovsky, M. A. Petruska, J. A. Hollingsworth, H. Htoon, M. G. Bawendi and V. I. Klimov, *Appl. Phys. Lett.*, 2002, **81**, 1303–1305.
40 J. Hare, S. Steiner, F. Orucevic and V. Lefevre-Seguin, Silica microspheres as high-Q microcavities for semiconductor quantum-dot lasers, in *Optoelectronic Integrated Circuits VII*, ed. L. A. Eldada and E. H. Lee, 2005, vol. 5729, pp. 94–103.
41 V. C. Sundar, H. J. Eisler, T. Deng, Y. T. Chan, E. L. Thomas and M. G. Bawendi, *Adv. Mater.*, 2004, **16**, 2137.
42 C. E. Finlayson, D. S. Ginger and N. C. Greenham, *Appl. Phys. Lett.*, 2000, **77**, 2500–2502.
43 F. Garcia-Santamaria, Y. F. Chen, J. Vela, R. D. Schaller, J. A. Hollingsworth and V. I. Klimov, *Nano Lett.*, 2009, **9**, 3482–3488.
44 J. Nanda, S. A. Ivanov, M. Achermann, I. Bezel, A. Piryatinski and V. I. Klimov, *J. Phys. Chem. C*, 2007, **111**, 15382–15390.
45 V. I. Klimov, S. A. Ivanov, J. Nanda, M. Achermann, I. Bezel, J. A. McGuire and A. Piryatinski, *Nature*, 2007, **447**, 441–446.
46 B. R. Walsh, J. I. Saari, M. M. Krause, R. Nick, S. Coe-Sullivan and P. Kambhampati, *J. Phys. Chem. C*, 2015, **119**, 16383–16389.
47 P. Kambhampati, *Acc. Chem. Res.*, 2011, **44**, 1–13.
48 R. R. Cooney, S. L. Sewall, D. M. Sagar and P. Kambhampati, *J. Chem. Phys.*, 2009, **131**, 164706.
49 P. Kambhampati, *J. Phys. Chem. Lett.*, 2012, **3**, 1182–1190.
50 R. R. Cooney, S. L. Sewall, D. M. Sagar and P. Kambhampati, *Phys. Rev. Lett.*, 2009, **102**, 127404.
51 C. H. Lin, E. Lafalce, J. Jung, M. J. Smith, S. T. Malak, S. Aryal, Y. J. Yoon, Y. Zhai, Z. Lin, Z. V. Vardeny and V. V. Tsukruk, *ACS Photonics*, 2016, **3**, 647–658.
52 M. Liu, Y. Ma and R. Y. Wang, *ACS Nano*, 2015, **9**, 12079–12087.
53 N. C. Anderson, M. P. Hendricks, J. J. Choi and J. S. Owen, *J. Am. Chem. Soc.*, 2013, **135**, 18536–18548.
54 M. M. Krause, L. Jethi, T. G. Mack and P. Kambhampati, *J. Phys. Chem. Lett.*, 2015, **6**, 4292–4296.
55 Sigma-Aldrich, ChemSpider, and Chemicalize for measured and theoretical thermodynamic data and geometry data for butylamine, octylamine, hexadecylamine, oleic acid, trioctylphosphane oxide, and pyridine.
56 W. K. Bae, K. Char, H. Hur and S. Lee, *Chem. Mater.*, 2008, **20**, 531–539.
57 W. K. Bae, M. K. Nam, K. Char and S. Lee, *Chem. Mater.*, 2008, **20**, 5307–5313.
58 Bellex International Coportation, Wilmington DE, USA. CYTOP chemical and physical properties. http://www.bellexinternational.com/products/cytop/.
59 C. Wurth, M. Grabolle, J. Pauli, M. Spieles and U. Resch-Genger, *Anal. Chem.*, 2011, **83**, 3431–3439.
60 M. E. McConney, S. Singamaneni and V. V. Tsukruk, *Polym. Rev.*, 2010, **50**, 235–286.
61 M. D. McGehee, R. Gupta, S. Veenstra, E. K. Miller, M. A. Diaz-Garcia and A. J. Heeger, *Phys. Rev. B: Condens. Matter Mater. Phys.*, 1998, **58**, 7035–7039.
62 P. Guyot-Sionnest, B. Wehrenberg and D. Yu, *J. Chem. Phys.*, 2005, **123**, 074709.
63 D. Choi, J. Y. Pyo, Y. Kim and D. J. Jang, *J. Mater. Chem. C*, 2015, **3**, 3286–3293.
64 P. Maity, T. Debnath and H. N. Ghosh, *J. Phys. Chem. C*, 2015, **119**, 10785–10792.
65 B. S. Kim, L. Avila, L. E. Brus and I. P. Herman, *Appl. Phys. Lett.*, 2000, **76**, 3715–3717.
66 D. I. Kim, M. A. Islam, L. Avila and I. P. Herman, *J. Phys. Chem. B*, 2003, **107**, 6318–6323.
67 G. Robert, Hunsperger, Integrated Optics, Theory and Technology, *Optical Waveguide Modes*, Springer Science and Business Media, 2009, ch. 2.
68 F. Todescato, I. Fortunati, S. Gardin, E. Garbin, E. Collini, R. Bozio, J. J. Jasieniak, G. Della Giustina, G. Brusatin, S. Toffanin and R. Signorini, *Adv. Funct. Mater.*, 2012, **22**, 337–344.
69 S. L. Sewall, R. R. Cooney, K. E. H. Anderson, E. A. Dias, D. M. Sagar and P. Kambhampati, *J. Chem. Phys.*, 2008, **129**, 084701.
70 S. Yang, Y. Wang and H. Sun, *Adv. Opt. Mater.*, 2015, **3**, 1136–1162.
71 M. Califano, *ACS Nano*, 2015, **9**, 2960–2967.
72 Y.-S. Park, W. K. Bae, J. M. Pietryga and V. I. Klimov, *ACS Nano*, 2014, **8**, 7288–7296.
73 W. K. Bae, Y.-S. Park, J. Lim, D. Lee, L. A. Padilha, H. McDaniel, I. Robel, C. Lee, J. M. Pietryga and V. I. Klimov, *Nat. Commun.*, 2013, **4**, 2661.

74 R. R. Cooney, S. L. Sewall, K. E. H. Anderson, E. A. Dias and P. Kambhampati, *Phys. Rev. Lett.*, 2007, **98**, 177403.
75 V. I. Klimov, A. A. Mikhailovsky, D. W. McBranch, C. A. Leatherdale and M. G. Bawendi, *Science*, 2000, **287**, 1011–1013.
76 M. Green, *J. Mater. Chem.*, 2010, **20**, 5797–5809.
77 C. R. Kagan, C. B. Murray and M. G. Bawendi, *Phys. Rev. B: Condens. Matter Mater. Phys.*, 1996, **54**, 8633–8643.
78 K. L. Shaklee and R. F. Leheny, *Appl. Phys. Lett.*, 1971, **18**, 475.
79 M. Segev, Y. Silberberg and D. N. Christodoulides, *Nat. Photonics*, 2013, **7**, 197–204.
80 C. Javaux, B. Mahler, B. Dubertret, A. Shabaev, A. V. Rodina, A. L. Efros, D. R. Yakovlev, R. Liu, M. Bayer, G. Camps, L. Biadala, S. Buil, X. Quelin and J. P. Hermier, *Nat. Nanotechnol.*, 2013, **8**, 206–212.
81 G. E. Cragg and A. L. Efros, *Nano Lett.*, 2010, **10**, 313–317.